Macromolecules

Article

pubs.acs.org/Macromolecules

Roles of Monomer Binding and Alkoxide Nucleophilicity in Aluminum-Catalyzed Polymerization of ε-Caprolactone

Keying Ding,[†,§] Maria O. Miranda,[†,§] Beth Moscato-Goodpaster,[†] Noureddine Ajellal,[†] Laurie E. Breyfogle,[†] Eric D. Hermes,[†] Chris P. Schaller,[‡] Stephanie E. Roe,[‡] Christopher J. Cramer,[†] Marc A. Hillmyer,[†,*] and William B. Tolman[†,*]

[†]Department of Chemistry, Center for Sustainable Polymers, and Supercomputing Institute, University of Minnesota, 207 Pleasant Street SE, Minneapolis, Minnesota 55455, United States

[‡]Department of Chemistry, College of St. Benedict/St. John's University, 37 South College Avenue, St. Joseph, Minnesota 56374, United States

Supporting Information

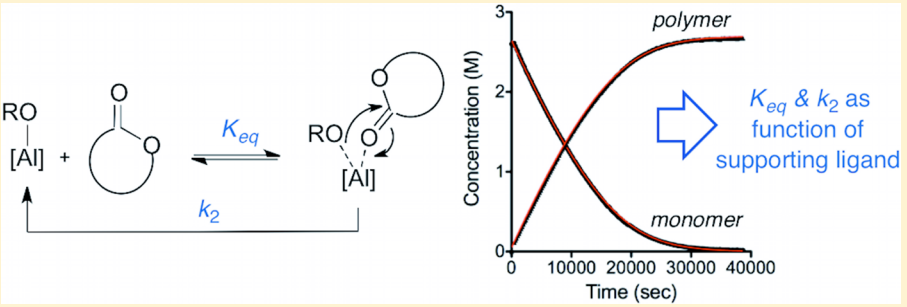

ABSTRACT: The kinetics of polymerization of ε-caprolactone (CL) initiated by aluminum-alkoxide complexes supported by the dianionic forms of *N*,*N*-bis[methyl-(2-hydroxy-3-*tert*-butyl-5-R-phenyl)]-*N*,*N*-dimethylethylenediamines, (L^R)Al(O*i*-Pr) (R = OMe, Br, NO_2) were studied. The ligands are sterically similar but have variable electron donating characteristics due to the differing remote (*para*) ligand substituents R. Saturation kinetics were observed using $[CL]_0$ = 2−2.6 M and $[complex]_0$ = 7 mM, enabling independent determination of the substrate coordination (K_{eq}) and insertion (k_2) events in the ring-opening polymerization process. Analysis of the effects of the substituent R as a function of temperature on both K_{eq} and k_2 yielded thermodynamic parameters for these steps. The rate constant k_2, related to alkoxide nucleophilicity, was strongly enhanced by electron-donating R substituents, but the binding parameter K_{eq} is invariant as a function of ligand electronic properties. Density functional calculations provide atomic-level detail for the structures of key reaction intermediates and their associated thermochemistries.

INTRODUCTION

The ring-opening polymerization (ROP) of cyclic esters is a key method for the synthesis of renewably derived and biodegradable materials, which are of interest for supplanting petroleum-derived plastics in a multitude of applications.[1−4] Metal alkoxide complexes are effective catalysts for ROP of a variety of cyclic esters,[1−5] of which ε-caprolactone (CL) and lactide (LA) are particularly well-studied examples. Improving the performance and versatility of metal-alkoxide catalysts is an important research goal that may be achieved through understanding the mechanism(s) of the ROP process and applying that knowledge to catalyst design and development. Metal alkoxide complexes are thought to operate by a "coordination−insertion" mechanism, whereby a Lewis acidic metal center binds and activates the monomer, rendering it susceptible to nucleophilic attack by a bound growing alkoxide chain (Figure 1). While a useful paradigm, this oft-cited picture is simplistic, and although some aspects of the bond making and breaking events have been discerned from theory,[6] detailed insights from experiment[7] are scant and sometimes contradictory.

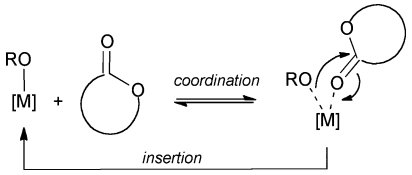

Figure 1. Coordination−insertion mechanism for cyclic ester ring-opening polymerizations.

For example, a number of workers have sought to address the role of metal ion Lewis acidity in ROP reactions.[8−16] Comparative studies of both bis(morpholinomethyl)phenoxy

Received: June 4, 2012
Revised: June 8, 2012

   dx.doi.org/10.1021/ma301130b | *Macromolecules* XXXX, XXX, XXX−XXX

and tris(pyrazolyl)hydroborate complexes have indicated that LA polymerization rates are enhanced in the presence of more electropositive metals (Ca > Mg > Zn).[14,15] Increasing electrophilicity of Zn(II) ions in complexes of neutral N-donor ligands has been correlated with higher activity in LA polymerizations.[16] The practice of modifying ancillary ligands has allowed for additional investigations in which electron donating and withdrawing groups are used to tune catalyst reactivity. Thus, studies of aluminum complexes of tetradentate salen- and salan-type ligands have shown enhanced LA polymerization rates with ligands that incorporate electron-withdrawing substituents such as chlorine.[8,10,11]

In contrast, we previously reported the catalytic polymerization of CL by aluminum alkoxide complexes and found that an electronegative bromine substituent on the supporting ligand retards the overall reaction rate.[17] Similarly, in LA polymerizations using a related aluminum system, slightly slower polymerization rates were reported for a complex supported by a ligand having chlorine instead of methyl substituents.[9] For LA polymerizations using a titanium salen catalyst the order of reactivity decreases as the ligand substituent becomes more electron withdrawing (MeO > alkyl > I > Cl).[12] Furthermore, in magnesium complexes employing phenolic benzenesulfonate ligands, increasing electronegativity of halogen substituents in the ligand also results in reduced reaction rates.[13]

The apparently variable effects of changing the Lewis acidity of the metal center on ROP reaction rates suggest that the sensitivity of the coordination and insertion steps to Lewis acidity may differ. A pronounced electronic effect on monomer binding is typically assumed, wherein factors that render the metal center more positively charged are postulated to result in stronger monomer binding and activation to give higher polymerization rates. However, increased Lewis acidity of the metal center may also induce stronger binding of the growing alkoxide chain to the metal, retarding transfer of the alkoxide to the carbonyl of the monomer. A clear understanding of how the coordination and insertion steps respond to perturbations of the electron density at the metal center through delineation of kinetic parameters for each step is needed. Yet metal-alkoxide promoted ROP reaction rates have only yielded composite propagation rate constants that include contributions from both coordination and insertion processes, complicating interpretation of kinetic and thermodynamic parameters.

Herein, we describe kinetics studies of CL polymerization by a series of well-characterized, monomeric Al complexes supported by ligands with virtually identical steric profiles but with different remote substituents having variable electron-donating characteristics. Under conditions of high initial concentrations of CL, we observed saturation behavior, and this has enabled the determination of binding and catalytic turnover rate constants and associated thermodynamic parameters as a function of ligand substituent. These data, in conjunction with DFT calculations, provide mechanistic knowledge and insights of general significance for metal alkoxide catalyzed ROP reactions critical for sustainable polymer synthesis.

RESULTS AND DISCUSSION

Synthesis and Characterization of Catalysts. Three Al alkoxide complexes **1**−**3** supported by ligands $(L^R)^{2-}$ (R = OMe, Br, NO_2 in the *para* position of the phenolate moiety) were prepared as outlined in Scheme 1. The syntheses of **1**[17] and **2**[17,18] (R = OMe, Br) were reported previously (including X-ray crystal structures of **1** and **2**). New derivative **3**[19] (R = NO_2) was characterized by ^{1}H NMR spectroscopy and CHN analysis.[20] The ligand syntheses employed a double Mannich condensation of the corresponding substituted phenols. Yields of the ligand precursors L^R were sensitive to the nature of the variable substituent, ranging from 20% for R = NO_2 to 80% for R = OMe. Unfortunately, the strongly electron donating *p*-amino derivatives, R = NMe_2 or NH_2, proved unattainable either through coupling with L^{Br} or reduction of L^{NO_2}.

Scheme 1. Synthesis of Ligands and Complexes Examined in This Study

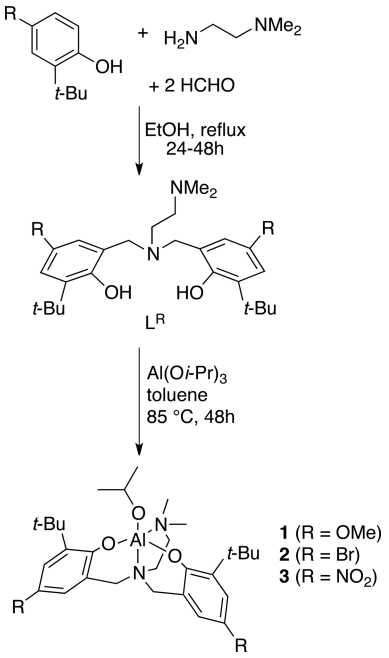

Coordination of the respective ligands to aluminum was effected through thermolysis of $Al(O\textit{i}\text{-}Pr)_3$ with equimolar amounts of the ligand in toluene (Scheme 1). Yields of complexes **1**−**3** were between 70 and 76%. The products were readily isolated as white (**1** and **2**) and pale yellow (**3**) solids by filtration, evaporation of volatiles and washing of the residues with cold pentane. The compounds are air- and moisture-sensitive, and soluble in aromatic hydrocarbons (toluene, benzene). In general, ^{1}H NMR spectra for **1**−**3** are quite similar; the only variations are the resonances associated with the *para*-substituent and chemical shift differences for the two aromatic protons adjacent to the *para*-substituent. All of the data support monomeric, 5-coordinate structures for the complexes as drawn in Scheme 1, with no evidence for aggregation in solution. Previously reported[21] pulsed gradient spin echo (PGSE) measurements for an analogous *tert*-butyl substituted ligand (R = *t*-Bu) in CD_2Cl_2 were consistent with this conclusion.[22]

Polymerization Kinetics Studies. In previously published work, all catalysts were shown to promote controlled polymerizations of CL to yield narrow molecular weight distribution ($Đ$ < 1.15) polycaprolactone (PCL) of prescribed molecular weights (M_n) that were a linear function of conversion and monomer-to-catalyst ratio.[17,19] Since all catalysts are similarly well-behaved, they are well-suited for kinetics studies.

dx.doi.org/10.1021/ma301130b | *Macromolecules* XXXX, XXX, XXX−XXX

The mechanism of the polymerization reaction proposed in Scheme 2 provides a framework for interpretation of

Scheme 2. Proposed Mechanism for CL Polymerization by Al Complexes

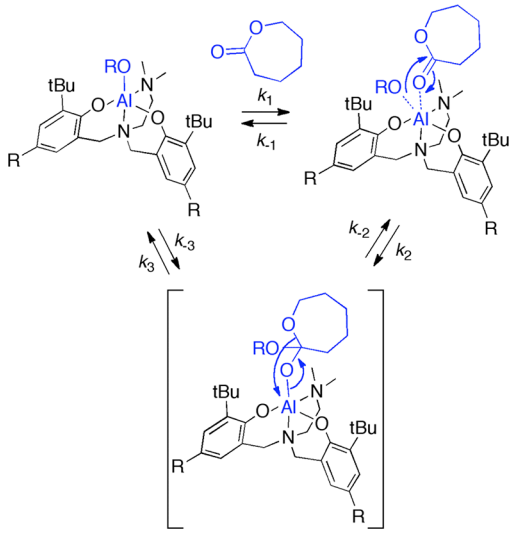

experimental kinetics data. With the caveat that assumptions about substrate binding and subsequent steps can be difficult to verify, we suggest that ROP involves reversible binding of a cyclic ester to the metal (k_1/k_{-1}), followed by transfer of an attached alkoxide to the activated carbonyl (k_2), and collapse of the resulting tetrahedral intermediate to reform the carbonyl and generate a new propagating alkoxide (k_3). The latter two steps are conceivably reversible. However, the considerably negative free energy change of ring-opening[23] suggests that the barrier for the ring-opening (k_3) would be lower compared to both ring-closing (k_{-3}) and alkoxide deinsertion (k_{-2}). On the basis of the general precedent for rapid collapse of the tetrahedral intermediate in the reactions of carboxylic acid derivatives, k_3 is probably post-rate determining. Thus, we simplify the mechanistic description to include only k_1, k_{-1}, and k_2. Accordingly, we anticipated that saturation kinetics could be observed at sufficiently high [CL] and that the Michaelis–Menten eq 1 (Al = complex **1**–**3**) would fit the data, ultimately enabling the determination of K_M and k_2 values. In addition, if binding is rapidly reversible, so that $k_{-1} \gg k_2$, K_M simplifies to the inverse of the binding constant (K_{eq}) between CL and the aluminum complex (eq 2).

$$-\frac{d[CL]}{dt} = \frac{d[PCL]}{dt} = \frac{k_2[Al][CL]}{K_M + [CL]} \quad (1)$$

$$K_M = \frac{k_{-1}}{k_1} = \frac{1}{K_{eq}} \quad (2)$$

To test this model, the progress of CL polymerizations catalyzed by **1**–**3** was evaluated by ^{1}H NMR spectroscopy. Reactions were performed in triplicate with a fixed initial concentration of monomer ($[CL]_0$ = 2.0–2.6 M) and catalyst ($[Al]_0$ = 7.0 mM) in toluene over a range of temperatures (18.5–80 °C).[24] Concomitant decay and growth of the resonances associated with the monomer and polymer were assessed and the concentrations of both as a function of time were modeled according to eq 1 by using COPASI (version 4.7.34),[25] a software package used for simulation and analysis of complex multistep equilibria in systems biology and for analysis of complex kinetics.[26] We also evaluated some of the data using a reaction progress kinetic analysis (RPKA) approach,[27] but chose to use COPASI for the complete study because (a) results using RPKA varied with the order of the polynomial used to fit the data (see Figures S10–S11, Table S2, Supporting Information), and (b) with COPASI, we were able to accurately and conveniently fit multiple species at once to solve for K_M and k_2. As an example, data for CL polymerization by **3** at 333 K with COPASI fits to eq 1 are shown in Figure 2. Additional

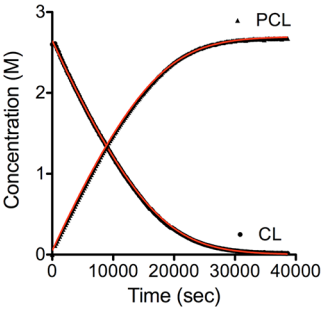

Figure 2. [CL] and [PCL] vs time data (●, ▲) and fit (red line) to eq 1 for polymerization of CL catalyzed by **3** at 333 K. Fit parameters: K_M = 1.046(9) M; k_2 = 0.0328(2) M^{-1} s^{-1}.

plots and tabulated K_M and k_2 values are provided as Supporting Information (Figures S3–S9, Table S1). The quality of the fits supports saturation behavior described by eq 1, and this conclusion is further corroborated by the inability to account for the concentration data using simpler first- or second-order rate laws (Figure S16, Supporting Information).

In addition to observing changes in [CL] and [PCL] by ^{1}H NMR spectroscopy during the course of the polymerization, we also noted changes in the aryl resonances of the catalyst as polymerization proceeded (Figures 3 and S12 (Supporting Information)). The two resonances separate from each other during the polymerization, such that the difference in chemical shift between the two peaks increases as [CL] decreases (moving from bottom to top of the stacked plot in Figure 3). To explain this phenomenon, we hypothesize that there is a rapid equilibrium between two complexes in solution that

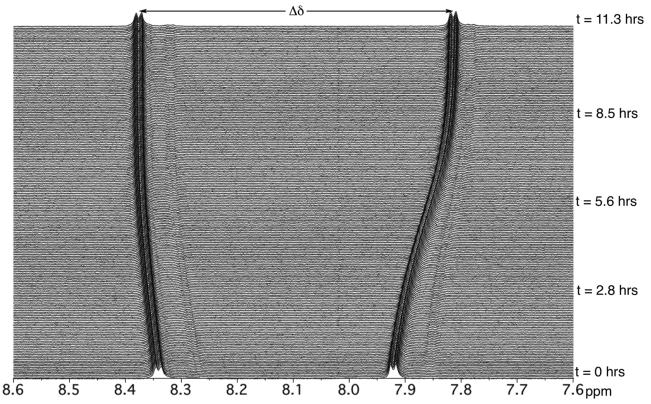

Figure 3. Portion of the ^{1}H NMR spectra acquired during the polymerization of CL by **3** at 333 K showing how the aryl resonances for the complex in solution change as a function of reaction time, as measured by the indicated peak separation Δδ.

dx.doi.org/10.1021/ma301130b | *Macromolecules* XXXX, XXX, XXX–XXX

involves CL, such that a single set of resonances are seen at each point in time but their relative peak positions shift as a function of [CL]. The simplest such equilibrium would be that involving CL binding to the catalyst, described by K_{eq}. Thus, by appropriate fitting of the aryl peak position separation ($\Delta\delta$) as a function of [CL], K_{eq} (or K_M, assuming $k_{-1} \gg k_2$) may be measured independently of the polymerization rate measurements, allowing the kinetic model for the polymerization to be tested. In this approach, we ignore the possibility of esters in the backbone of PCL binding to the catalyst and assume that at the end of the reaction, the catalyst is in an unbound state. This is consistent with the general inability of Al-based alkoxides to effect polymer transesterification.

Since for two species in rapid equilibrium the observed chemical shift is equal to the average of the chemical shifts for the two distinct species, weighted by their concentrations, and under the assumption that eq 1 applies, the relationship in eq 3 between the chemical shift difference between the aryl resonances, $\Delta\delta$, and [CL] may be derived, where $\Delta\delta_{uncoord}$ is the peak position difference for the catalyst that is not bound to CL and $\Delta\delta_{coord}$ is the peak position difference for the species bound to CL (see Supporting Information for the derivation of eq 3).

$$\Delta\delta = \Delta\delta_{uncoord} + \frac{(\Delta\delta_{uncoord} - \Delta\delta_{coord})[CL]}{K_M + [CL]} \quad (3)$$

Plots of $\Delta\delta$ versus [CL] were fit using a nonlinear regression to eq 3 and K_M values were determined, as illustrated in Figure 4 for one experiment using **3** at 333 K. Results from the same

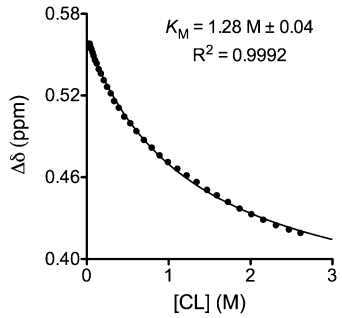

Figure 4. Plot of $\Delta\delta$ from the NMR spectra in Figure 3 versus [CL] during the polymerization of CL, with the fit to eq 3.

analysis of data acquired at other temperatures and for experiments using **2** are provided as Supporting Information (Figures S13–S14); due to spectral overlap issues this analysis was not possible for **1**. For the case of **3**, the K_M values determined from the separate NMR and kinetic analyses were in close agreement (cf. at 323 K, K_M (NMR) = 1.15 ± 0.03 M, K_M (COPASI avg) = 0.962 ± 0.009 M), while for **2** they were within a factor of 4 (at 323 K, K_M (NMR) = 1.8 ± 0.1 M, K_M (COPASI avg) = 0.55 ± 0.01 M, Figure S15, Table S3, Supporting Information). Note, however, that this latter difference corresponds to a $\Delta\Delta G^\circ$ < 1 kcal/mol, on the order of experimental error (see discussion of thermodynamics below). Importantly, the agreement between the K_M values determined by the two independent methods provides further support for the mechanistic picture shown in Scheme 2 and the validity of eq 1.

Isolation of a Complex after Polymerization. After polymerization experiments using **3** were completed and the NMR tubes were allowed to stand in air at room temperature for several days, crystals were observed within the polymer solution in the tubes. An X-ray crystal structure determination was performed that showed the crystals to comprise the dinuclear complex **4** (Figure 5). The complex contains two

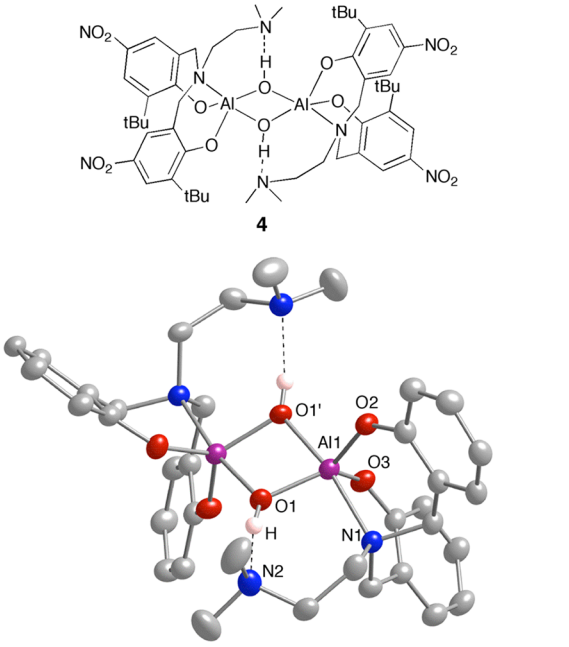

4

Figure 5. Line drawing of complex **4** (top), and representation of the X-ray crystal structure of **4**, showing 50% thermal ellipsoids with all hydrogen atoms (except those on the bridging hydroxo groups) and *tert*-butyl and $-NO_2$ substituents omitted for clarity (bottom). Selected interatomic distances (Å) and angles (deg) are as follows: Al1–O1, 1.7859(14); Al1–O1′, 1.8626(14); Al1–O2, 1.7702(14); Al1–O3, 1.7733(14); Al1–N1, 2.1253(16); Al1–Al1′, 2.8007(11); O1–H, 0.80(2); N2–H, 1.865; O1–N2, 2.658; O1–Al1–O2, 125.69(7); O1–Al1–O3, 119.25(7); O1–Al1–N1, 92.46(6); O1–Al1–O1′, 77.96(7); O2–Al1–O3, 114.99(7); O2–Al1–N1, 90.90(6); O2–Al1–O1′, 97.50(6); O3–Al1–N1, 89.13(6); O3–Al1–O1′, 92.52(6); N1–Al1–O1′, 169.81(6); Al1–O1–Al1′, 100.26(7); Al1–O1–H, 126.2(15); Al1–O1′–H′, 133.5(15); O1–H–N2, 170.13.

symmetry-related Al centers, each ligated in tridentate fashion by $(L^{NO_2})^{2-}$. The dimethylamino arms of the ligand are not complexed to the metal, and instead are hydrogen-bonded to hydroxides that bridge the Al sites. These sites adopt slightly distorted trigonal bipyramidal geometries (τ = 0.74),[28] with the trigonal plane including three oxygen atoms, two from the phenoxides on the ligand (O2, O3) and one from a bridging hydroxide (O1). The nitrogen (N1) and the other bridging hydroxide moiety (O1′) are the axial donors (N1–Al1–O1′ = 169.80°). The Al–O and Al–N interatomic distances are similar to those reported previously for complexes **1**, **2**, and an analogue featuring $(L^{tBu})^{2-}$.[17,18] We surmise that the hydroxide ligands derive from water impurities introduced during or after the polymerization, although we have not explored this issue in detail. Importantly, the identification of **4** provides unequivocal precedence for the notion that the dimethylamino arm of $(L^R)^{2-}$ can dissociate from an Al(III) center, which may occur during polymerization catalysis (see below).

Rate Constants and Mechanistic Interpretations. Turning first to analysis of k_2, its dependencies on ligand substituent R and temperature are revealed in plots of log(k_2)

dx.doi.org/10.1021/ma301130b | *Macromolecules* XXXX, XXX, XXX–XXX

vs σ_p[29] (Figure 6, top) and $\ln(k_2/T)$ vs $1/T$ (Figure 6, bottom). Linear correlations between substituent electronic parameters

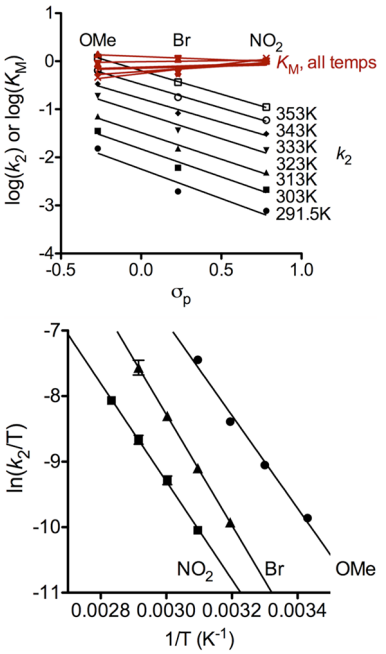

Figure 6. Hammett plot (top) for k_2 (black) and K_M (red) and Erying plot (bottom) for k_2 for catalysts **1** (circle), **2** (triangle), and **3** (square).

and k_2 were observed at all temperatures and essentially invariant negative ρ values (slopes) were found (average ρ = −1.1(1)).[30] Clearly, increasing the electron-donating capability of the *para*-substituent significantly enhances the insertion step, and the linear correlation supports an invariant mechanism across the series. The trend may be rationalized by invoking a prominent role played by binding of the alkoxide nucleophile in this system: more electron-donating ligands render the alkoxide more labile and more reactive, presumably through decreasing the Lewis acidity of the metal and thus the strength of the Al−OR interaction.

Further insights into the insertion process are provided by the activation parameters determined from the Eyring plots for k_2 (Figure 6, bottom; Table 1). In general, modest activation

Table 1. Activation Parameters Associated with k_2

complex	R	$\Delta H^{\ddagger}$ (kcal/mol)	$\Delta S^{\ddagger}$ (cal/mol K)	$\Delta G^{\ddagger}$ (kcal/mol, 323 K)
1	OMe	14.1 ± 0.5	−19 ± 1	20.1 ± 0.6
2	Br	16.8 ± 0.3	−13.3 ± 0.4	21.1 ± 0.3
3	NO_2	14.9 ± 0.5	−21.0 ± 0.7	21.7 ± 0.4

enthalpies accompany negative activation entropies. The parameters imply a moderate degree of bond breaking and ordering in going to the transition state, consistent with a concerted transfer of the metal-bound alkoxide to the coordinated carbonyl with cleavage of the carbonyl π bond.

Considering next K_M, one encounters a different situation. At all temperatures and for all catalysts, plots of $\log(K_M)$ vs σ_p (Figure 6, top) give slightly positive average ρ values of +0.1(2) that are effectively close to zero, indicating that the equilibrium is insensitive to substituents. Surprisingly, it appears as though monomer binding is unaffected by the electronic nature of the ligand, and therefore the electrophilicity at the metal center. This observation is further supported by the thermodynamic data, which for ease of interpretation are plotted in Figure 7 as

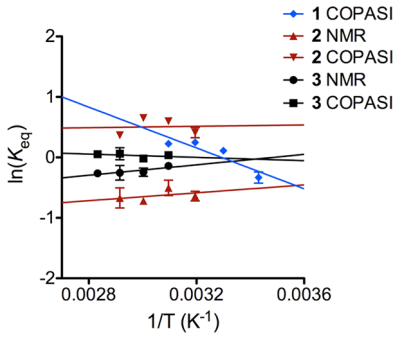

Figure 7. Van't Hoff plot for K_{eq} for catalysts **1** (blue), **2** (red), and **3** (black). The designation NMR or COPASI indicates which analysis method (*vida supra*) was used to obtain the data. NMR: NMR peak analysis method. COPASI: kinetic analysis using COPASI.

$\ln(K_{eq})$ vs $1/T$, with the assumption that $K_M^{-1} = K_{eq}$; thermodynamic parameters derived from K_{eq} are listed in Table 2. Excellent agreement between the parameters

Table 2. Thermodynamic Parameters Associated with K_{eq} As Determined by COPASI and NMR Peak Analysis Methods

complex	method	R	ΔH° (kcal/mol)	ΔS° (cal/molK)	ΔG° (kcal/mol, 323 K)
1	COPASI	OMe	3.3 ± 0.5	11 ± 2	−0.2 ± 0.8
2	COPASI	Br	−0.1 ± 0.8	0.6 ± 2	−0.3 ± 1
2	NMR	Br	−0.6 ± 1	−3 ± 3	0.4 ± 1
3	COPASI	NO_2	0.3 ± 0.4	0.9 ± 1	−0.01 ± 0.8
3	NMR	NO_2	−0.9 ± 0.3	−3 ± 1	0.1 ± 0.5

determined independently from the kinetic analysis and the analysis of the NMR resonances for the Al complex during polymerization supports the validity of the overall mechanistic model and a rapid pre-equilibrium before monomer insertion. Again, these plots all have slopes of essentially zero, and have standard Gibbs free energies of nearly zero. In the case of **1**, the small, positive enthalpy change and positive entropy change support a dissociative interchange process,[31] indicating a possible ligand rearrangement occurring simultaneously with monomer binding.

To rationalize the monomer binding thermodynamics for the complexes supported by electron donating and withdrawing ligands, we propose different pathways for each type of system, which may operate in parallel (Scheme 3). In one pathway (**A**), an amine arm of the ligand dissociates, opening up a vacant coordination site. Monomer then approaches the resulting four-coordinate aluminum complex, which is less sterically crowded than its precursor, and binds to form a pentacoordinate intermediate. This route would be favored in complexes with electron-donating substituents (i.e., **1**) that can stabilize a lower-coordinate aluminum intermediate. Increasing temperature would promote dissociation of the ligand arm, as reflected in the positive ΔS° associated with K_{eq}, and facilitate monomer binding and reaction. In a second pathway (**B**), monomer coordinates to the aluminum complex directly to form an octahedral intermediate. This pathway would be favored for the complexes with electron withdrawing ligands (i.e., **2** and **3**), for which dissociation of the ligand arm is retarded by the

dx.doi.org/10.1021/ma301130b | *Macromolecules* XXXX, XXX, XXX−XXX

Scheme 3. Proposed Mechanisms for Binding of CL to Catalysts 1−3

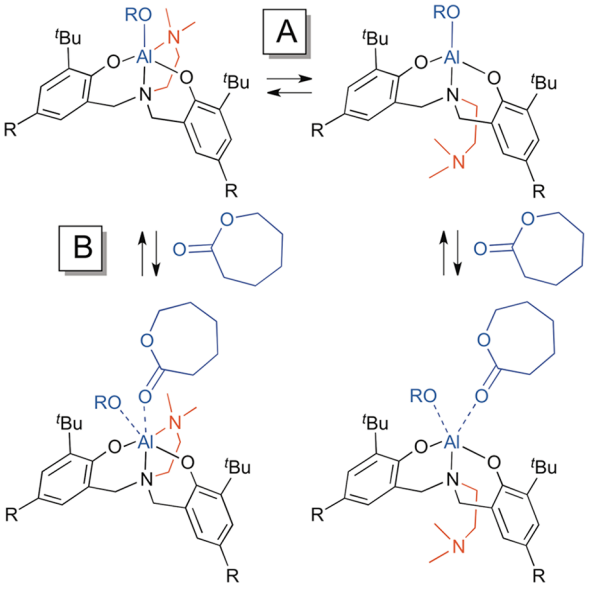

enhanced Lewis acidity of the metal. In these complexes, increasing temperature has little effect on binding of the monomer.

The amine arm dissociation central to the above hypothesized mechanistic scheme is supported by several lines of evidence. Precedence comes from a report describing this phenomenon for a vanadium complex of $(L^{tBu})^{2-}$,[32] proposed involvement of amine arm dissociation in ROP catalysis by zinc catalysts,[33] and the X-ray structure of **4**. In addition, we performed variable temperature (VT) NMR studies on **1** (toluene-d_8, 500 MHz) with and without exogenous pyridine, the binding of which would mimic coordination of CL during polymerization. In the absence of added pyridine, several peaks in the ^{1}H NMR spectrum measured at room temperature reversibly decoalesced to separate signals upon cooling (Figure S17, Supporting Information). For example (Figure 8a), single peaks in the room temperature spectrum for the amine-arm methyl groups (NMe_2) and the methoxy aryl substituents convert to two separate resonances at 192 K (coalescence temperatures ∼230−235 K). The low temperature spectrum is consistent with a static C_s symmetric geometry for the complex as found in its X-ray crystal structure.[17] Peak coalescence and simplification of the spectrum upon warming reflects a fluxional process that averages the chemical environment of the ligand hydrogen atoms, presumably via interconversion of ligand conformers (e.g., chelate "ring flips").

In the presence of excess pyridine (50 equiv), only free pyridine and an averaged set of peaks for **1** are apparent in the NMR spectrum measured at 292 K (Figures 8b and S18, Supporting Information). Upon cooling, however, changes in the spectrum occur that support binding of pyridine and displacement of the amine-arm of the supporting ligand (Scheme 4). Notably, at 192 K a peak for coordinated pyridine appears at δ 9.4 ppm, ∼0.8 ppm downfield from free pyridine, and a singlet for the NMe_2 group appears at δ 2.0 pm, at the same position as in the free (uncoordinated, protonated) ligand. With 1 equiv of pyridine, the identical set of peaks assigned to the pyridine adduct are seen at 192 K, in conjunction with those associated with **1** alone (Figure S19,

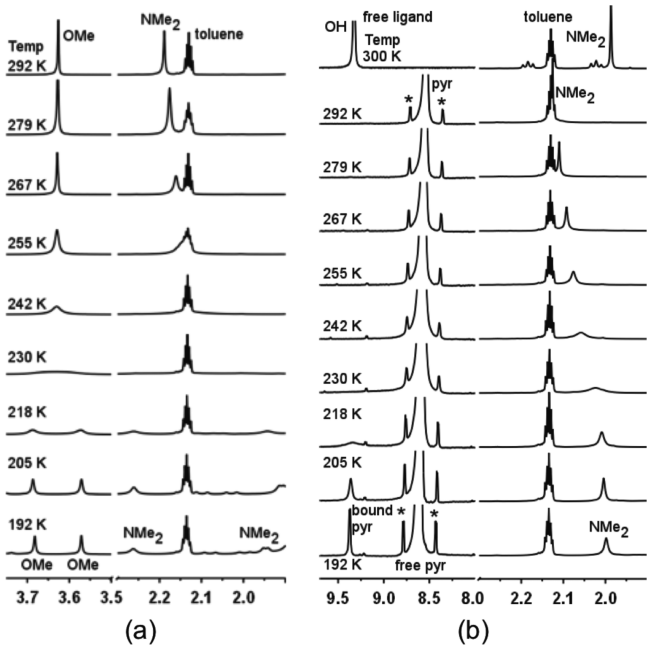

Figure 8. Portions of the VT ^{1}H NMR spectra of complex **1** in toluene-d_8 (a) with no added reagents, and (b) in the presence of 50 equiv of pyridine (pyr). The spectrum of the free (uncoordinated, protonated version) of the ligand is shown for reference at the top of the stacked plot in part b. Asterisks denote spinning side-bands associated with the free pyr resonance.

Scheme 4. Proposed binding of pyridine to complex 1

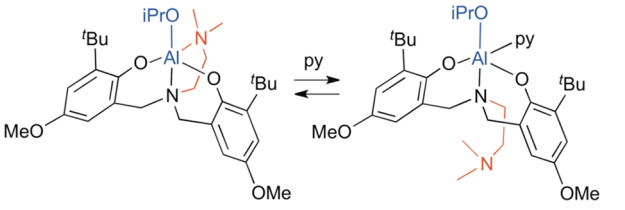

Supporting Information). In sum, the VT NMR data in the presence of pyridine support lability of the dimethylamino arm, as proposed in Scheme 3.

To further evaluate the mechanism shown in Scheme 3, we carried out density functional calculations on the complexes with and without coordination of the amine arm and with and without bound CL. The nature of the catalyst, the alkoxide, and CL is such that substantial conformational diversity is possible, but representative structures are presented in Figure 9 for L^H for simplicity (calculations were done for complexes **1**−**3**). In the absence of CL binding, the coordination geometry about Al is roughly tetrahedral when the amine arm is decoordinated (Figure 9d) and roughly trigonal bipyramidal when the amine arm is coordinated (Figure 9c). The enthalpy cost to decoordinate the amine arm is predicted to range from 16.4 kcal/mol for L^{OMe} to 19.2 kcal/mol for L^{NO_2} (Table 3; compare the mono-RO arm-off column to the mono-RO arm-on column). Considering the *free energies* of arm decoordination at 333 K (not tabulated), values for all three ligands are predicted to be about 3 kcal/mol less positive than the enthalpies of decoordination. However, the magnitude of the entropic contribution favoring decoordination is likely underestimated. Identification of all of the relevant arm-off and arm-on conformational isomers is not practical due to their sizes,

dx.doi.org/10.1021/ma301130b | *Macromolecules* XXXX, XXX, XXX−XXX

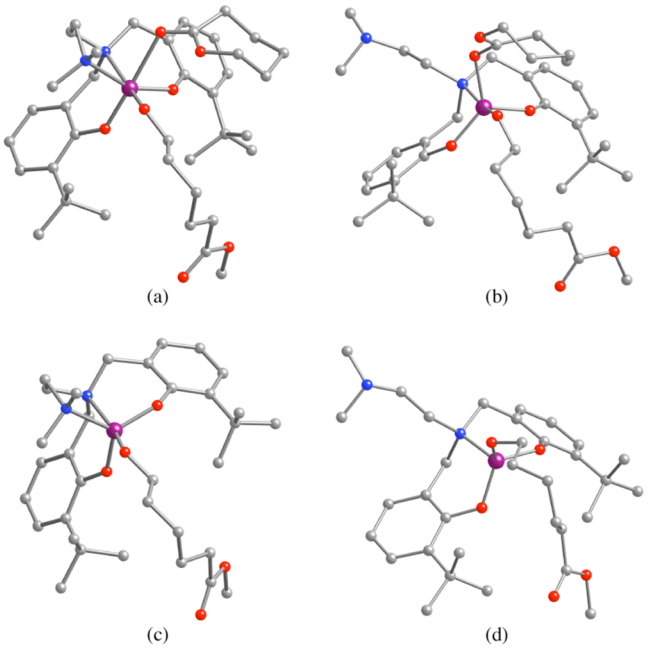

Figure 9. Ball-and-stick stereostructures of representative $L^{H}AlOR$ (R = $(CH_2)_5CO_2Me$) complexes with L^{H} coordinated in tetradentate (a, c) and tridentate (b, d) fashion, with (a, b) and without (c, d) coordinated ε-caprolactone. All structures were fully optimized at the DFT level of theory (see Theoretical Methods). Hydrogen atoms are not shown for clarity, carbon atoms are gray, nitrogen atoms are blue, oxygen atoms are red, and aluminum atoms are purple. The illustrated structures are designated Mono-RO in Table 5. Structures in which the terminal ester of the alkoxide ligand also coordinate Al, designated Bi-RO in Table 5, are higher in enthalpy than those shown here.

Table 3. Relative 333 K Enthalpies (kcal/mol) of Different Catalyst Structures with and without Bound CL[a]

	arm-off			arm-on		
p-subst	bi-RO[b]	mono-RO[c]	mono-RO/CL[d]	bi-RO[b]	mono-RO[c]	mono-RO/CL[d]
OMe	21.6	16.4	7.7	6.8	0.0	−3.1
Br	20.9	17.8	7.5	5.0	0.0	−4.9
NO_2	20.0	19.2	6.8	2.2	0.0	−8.5

[a]Monocoordinated alkoxide and infinitely separated CL. [b]Enthalpies computed as sum of M06-L/6-31G(d) thermal contributions (see Theoretical Methods) and SMD(toluene)/M06-2X/6-311+G(d)//M06-L/6-31G(d) electronic energies for structures analogous to those shown in Figure 5, i.e., not accounting for potentially large populations of conformational isomers within each structural class. [c]Bidentate alkoxide/ester and infinitely separated CL. [d]Monocoordinated alkoxide with bound CL.

but the decreased steric congestion around aluminum in the arm-off case would be expected to permit a substantially larger number of conformers to exist at low energy compared to the arm-on alternative. This would contribute to even more entropic lowering of the population free energy in the arm-off case.

We evaluated the tendency for the propagating alkoxide itself to act as a bidentate ligand, through the coordination of its ester carbonyl to Al. We have located such structures (not shown) and in the arm-off case, they are enthalpically less stable than their monocoordinated alkoxide antecedents by from 5.2 (L^{OMe}) to 0.8 (L^{NO_2}) kcal/mol. In the arm-on case, the enthalpic preference for monocoordination increases in every case by about 2 kcal/mol; the direction of this change is as expected given the decreased Al electrophilicity that results from coordination of the amine functionality. Entropic considerations for individual 333 K structures like those shown in Figure 5 further destabilize the bidentate structures by 3 to 4 kcal/mol in free energy (not tabulated). As noted above, such an estimate is likely somewhat too low given the flexibility of the alkoxide chain when it is monocoordinated compared to bound in a bidentate fashion. In any case, there appears to be no strong bias for a growing polymer chain to block the approach of new monomer to the catalytic center.

The arm-on and arm-off structures with bound CL have roughly octahedral and trigonal bipyramidal coordination about the aluminum atom, respectively (Figure 9, parts a and b). If we consider the enthalpies of complexation of CL to the catalyst, in the arm-off case the complexation is exothermic by −12.4 kcal/mol for L^{NO_2} and −8.7 kcal/mol for L^{OMe} (of course, it is predicted to be *endo*thermic to decoordinate the amine, but comparing data columns 2 and 3 of Table 3 permits us to quantify the enthalpy of CL coordination subsequent to arm *de*coordination). The same complexation enthalpies range from −8.5 to −3.1 kcal/mol when the amine arm remains coordinated (final two data columns of Table 3). As expected, the exothermicities are smaller, and the range of variation is smaller, when the coordinated amine decreases the Al Lewis acidity. We may also compare the enthalpic cost to decoordinate the amine arm *after* CL complexation: it ranges from 15.3 kcal/mol for L^{NO_2} to 10.8 kcal/mol for L^{OMe}. We note that these are clearly upper bounds as coordination of a toluene solvent molecule to a vacant Al site may reduce these enthalpic costs, and this effect is not included in the calculations.

While it is tempting to compare the *measured* enthalpies of complexation in Table 2 with the computed enthalpies of complexation in Table 3, the complexity of the experimental situation does not permit such a straightforward comparison. Over the temperature range studied experimentally, the apparent complexation enthalpies (and entropies) reflect averages over populations of arm-on and arm-off conformers that are themselves varying with temperature. In so far as none of the experimental ligands has an enthalpy of binding sufficiently negative to suggest that it exists solely as a population of arm-on conformers over the whole temperature range, it is not possible to use the theoretical data to make predictions about the apparent van't Hoff parameters in the absence of much more reliable estimates for entropy changes than can be obtained from the usual ideal-gas, rigid-rotator, harmonic-oscillator approximations that are typically combined with electronic structure calculations to estimate solute partition functions. Taken as a whole, however, the density functional predictions provide good support for the experimental interpretation of arm-on and arm-off isomers contributing differentially to the equilibrium populations of many of the studied catalyst−CL complexes, and in particular suggest that arm decoordination will be much more facile for the L^{OMe} ligand whether before or after CL complexation.

SUMMARY AND CONCLUSIONS

Through the use of ^{1}H NMR spectroscopy, saturation kinetics in the polymerization of CL by a series of Al catalysts was measured, thus enabling dissection of the typically observed composite propagation constant into separate insertion (k_2) and monomer binding (K_{eq}) parameters. By analysis of the

dx.doi.org/10.1021/ma301130b | *Macromolecules* XXXX, XXX, XXX−XXX

trends in these parameters as a function of the electronic characteristics of remote supporting ligand substituents and temperature, thermodynamic information on the separate insertion and monomer binding steps was obtained. The overall slower rates observed for complexes with electron withdrawing substituents is seen to derive entirely from k_2, as reflected by an average $\rho = -1.1(1)$ in $\log(k_2)$ vs σ_p plots over a range of temperatures. Analysis of activation parameters for k_2 show that entropic effects are predominant determinants of the trends in the rate constants. The trends in K_{eq} as a function of substituent and temperature are more complicated, with changes in thermodynamic parameters that we interpret as deriving from populations of species both pre- and post-complexation that consist of structures having either a bound or unbound dimethylamino arm (Scheme 3). Variable temperature NMR data acquired for complex **1** both with and without added pyridine, the binding of which models CL coordination during catalysis, are consistent with lability of the dimethylamino arm. Results from theory support the hypothesis that amino decoordination is less enthalpically unfavorable with ligands substituted by electron-donating groups, and such decoordination is evidently more important to binding over the temperature range examined here based on the more positive apparent entropy of complexation determined from van't Hoff analysis.

While the mechanistic insights provided herein are unique to the particular catalyst system studied and for polymerization of one lactone, CL, they nonetheless have important broader implications for how other catalysts might operate and for the design of new ones, particularly in view of the general significance of catalytic syntheses of sustainable materials.[1−5] Electronic variation of supporting ligand substituents clearly can have multiple influences during a polymerization process, and it would appear that differences in the relative importance of these influences (i.e., on insertion and substrate coordination) likely underlie the contradictory rate trends that have been observed in the literature. These factors can be understood through dissection of what are usually composite propagation rate constants, an approach that has much promise for future studies of catalysts other than those studied herein.

EXPERIMENTAL SECTION

General Considerations. All reactions were carried out under an inert atmosphere using standard Schlenk and drybox techniques, unless otherwise indicated. Reagents were obtained from commercial suppliers and used as received unless otherwise indicated. CL was purified by distillation from CaH_2 and stored under N_2. Deuterated solvents were dried over CaH_2 or sodium, distilled under vacuum and stored under N_2. Protiated solvents were degassed and passed through a solvent purification system (Glass Contour, Laguna, CA) prior to use. The ligands[17,34] and complexes with R = OMe and Br, as well as 2-*tert*-butyl-4-nitrophenol[35] were prepared by published methods. ^{1}H NMR spectra were recorded on a Varian VI-300 NMR spectrometer and their chemical shifts (δ) for ^{1}H spectra are referenced to residual protium in the deuterated solvent. Variable low-temperature NMR studies were performed on a Bruker Avance III 500 MHz spectrometer equipped with a BBFO SmartProbe. The temperature of the probe was calibrated using a methanol standard.

***N,N*-Bis[methyl-(2-hydroxy-3-*tert*-butyl-5-nitrophenyl)]-*N,N*-dimethylethylenediamine (L^{NO_2}).** 2-*tert*-Butyl-4-nitrophenol (3.1245 g, 16 mmol), *N,N*-dimethylethylenediamine (0.88 mL, 8.1 mmol), paraformaldehyde (0.6349, 21.1 mmol), and 50 mL of absolute ethanol were added to a 350 mL screw cap bomb flask. The flask was sealed and heated to 125 °C and allowed to react for 24 h. After allowed the flask to come to room temperature, the flask was opened in air and cooled to −20 °C. A precipitate formed and was filtered over a glass frit and washed with ice-cooled methanol (50 mL). The product was dissolved in minimum CH_2Cl_2 and recrystallized from ethanol at 0 °C to give an off white powder (0.7840 g, 20%). ^{1}H NMR (300 MHz, CD_2Cl_2): δ 8.11 (d, 2H, J = 2.7 Hz), 7.90 (d, 2H, J = 2.7 Hz), 3.71 (s, 4H), 2.69 (s, 4H), 2.37 (s, 6H), 1.38 (s, 18H). Anal. Calcd for $C_{26}H_{38}N_4O_6$: C, 62.13; H, 7.62; N, 11.15. Found: C, 62.23; H, 7.78; N, 11.13.

(L^R)Al(O*i*Pr) (3, R = NO_2). In a nitrogen-filled glovebox, an oven-dried 15 mL screw cap bomb flask was charged with aluminum isopropoxide (125.1 mg, 0.61 mmol), *N,N*-bis[methyl-(2-hydroxy-3-*tert*-butyl-5-nitrophenyl)]-*N′,N′*-dimethylethylenediamine (309.3 mg, 0.62 mmol), and 3 mL of toluene. The flask was sealed, removed from the glovebox, heated to 85 °C and allowed to stir for 2 days. After the reaction time had completed, the flask was cooled and returned to the glovebox. A precipitate had formed upon cooling. The toluene was removed *in vacuo*, and the remaining off-white powder was triturated three times with 5 mL of pentane. The product was recrystallized from CH_2Cl_2 and pentane (243.4 mg, 70%). ^{1}H NMR (300 MHz, CD_2Cl_2): δ 8.15 (d, 2H, J = 3.0 Hz), 7.86 (d, 2H, J = 3.0 Hz), 4.63 (septet, 1H, J = 5.7 Hz), 3.76 (app d, 2H, J = 13.2 Hz), 3.56 (app d, 2H, J = 13.2 Hz), 2.79 (m, 4H), 2.67 (s, 6H), 1.43 (s, 18H), 1.20 (d, 6H, J = 6 Hz). Anal. Calcd for $C_{29}H_{43}AlN_4O_7$: C, 59.37; H, 7.39; N, 9.55. Found: C, 58.60; H, 7.10; N, 9.28.

^{1}H NMR Kinetic Analyses. A representative procedure for the kinetic studies is described. To an oven-dried NMR tube in a nitrogen filled glovebox, 500 μL of a stock solution of catalyst in toluene-d_8 (0.0092M) and 10 μL of the internal standard bis(*p*-trimethylsilyl)-benzene in toluene-d_8 (0.28M) were added. The NMR tube was capped with a septum and wrapped with parafilm. A gastight syringe was loaded with 190 μL of ε-caprolactone (CL) stock solution (7.4 M), also in toluene-d_8. The target final concentrations of catalyst, internal standard, and CL were 0.007, 0.004, and 2 M, respectively. The gastight syringe containing CL was inserted into a rubber septum to prevent air contamination during the experiment setup. The NMR tube and syringe were removed from the glovebox and brought to the spectrometer. The temperature on the NMR spectrometer (300 MHz Varian Inova) was calibrated using an ethylene glycol standard. The catalyst and internal standard mixture was calibrated to a 30° pulse width, and a ^{1}H NMR spectrum was taken with the calibrated 30° pulse width, spin rate of 16 Hz, and delay time of 10 s to obtain accurate catalyst integrations. Next, the tube was ejected from the spectrometer and CL was injected through the septum into the NMR tube. The contents of the tube were well mixed before reinserting the NMR tube into the spectrometer. Using the previously calibrated 30° pulse width, an arrayed set of spectra were taken at 96, 192, or 384 s with 8, 16, or 32 scans, respectively, spin rate of 16 Hz, acquisition time 2 s, and a delay time of 10 s to ensure accurate integrations. The gain was adjusted such that it was as high as possible. The arrayed experiment was allowed to proceed until polymerization had completed (monitored by the disappearance of the CL residues). For each catalyst, four temperatures were carefully chosen, and three reactions were repeated at that temperature. The obtained arrayed NMR data were phased and baseline corrected before being integrated by Mestrenova (a chemistry software for NMR analysis, http://mestrelab.com/). The integrations were recorded and entered into an Excel spreadsheet. Absolute concentrations of all species as a function of time were computed relative to the concentration of internal standard. Reaction time was calculated in seconds from the known length of time per spectrum. For the RPKA analysis, the kinetic parameters were extracted from the time-dependent concentration data by fitting to an arbitrary nth order polynomial function (e.g., a ninth order polynomial, $[CL] = a_0 + a_1t + ... + a_9t^9$) and differentiating this function with respect to time ($d[CL]/dt = a_1 + 2a_2t + ... + 9a_9t^8$) to obtain instantaneous rate data. Kinetic parameters were determined by best fit to the Michaelis−Menten equation, (eq 1) and are listed in Table S2 (Supporting Information); representative fits are shown in Figures S10 (Supporting Information). For the COPASI analysis, the concentration vs time data obtained from the ^{1}H NMR data were input into COPASI program and fitted with Michaelis−Menten model

(eq 1) to obtain K_M and k_2 values. COPASI fitting plots (concentration vs time) are shown in Figures S3−S8, Supporting Information. The reaction rates were calculated by eq 1 and plotted as a function of concentration, as shown in Figure S9, Supporting Information. Kinetic parameters determined by COPASI are listed in Table S1, Supporting Information. All linear and nonlinear curve fits were performed using Graphpad Prism or Origin software.

Theoretical Methods. Gas-phase geometries were fully optimized at the density functional level of theory making use of the M06-L functional,[36] the 6-31G(d) basis set,[37] and an additional automatically generated density fitting basis set employed to speed integral evaluation. All structures were characterized as local minima from computation of analytic vibrational frequencies, which were also used to construct 333 K molecular partition functions using the ideal-gas, rigid-rotator, harmonic-oscillator approximation.[38] In the vibrational partition function, all frequencies below 50 cm^{-1} were replaced with a value of 50 cm^{-1} to correct for the inadequacy of the harmonic-oscillator approximation for such normal modes, and thermochemical contributions to enthalpies and entropies were computed from the resulting M06-L partition functions.[38]

The thermochemical contributions were added to single-point energies computed with the M06-2X functional[39] and the 6-311+G(d,p) basis set.[37] The M06-2X functional is particularly appropriate for these large, primarily organic architectures, where dispersion interactions between bulky groups may play a key role in stabilizing particular geometries and complexes.[40] The single point M06-2X calculations also included the effects of toluene solvation with the SMD continuum solvation model.[41] All thermochemistries are reported for a standard state of 1 M (consistent with the usual experimental convention).[38] We assume that the computed free energies of solvation are dominated by enthalpic effects, and thus include them in full in both reported enthalpies and free energies in discussion.

All calculations were accomplished with the Gaussian 09 electronic structure program suite.[42]

■ ASSOCIATED CONTENT

Ⓢ Supporting Information

Representative data, kinetic plots, derivation of eq 3, description of error analysis, and tabulated kinetics results and X-ray crystallographic data in format. This material is available free of charge via the Internet via http://pubs.acs.org.

■ AUTHOR INFORMATION

Corresponding Author

*E-mail: (W.B.T.) wtolman@umn.edu; (M.A.H.) hillmyer@umn.edu.

Author Contributions

[§]These two coauthors contributed equally to the work and should be considered cofirst authors.

Notes

The authors declare no competing financial interest.

■ ACKNOWLEDGMENTS

We thank the National Science Foundation (CHE-0610183 and -0952054 to C.J.C, -0842654 to W.B.T. and M.A.H. and a Graduate Research Fellowship under Grant No. 00006595 to M.O.M.) and the Center for Sustainable Polymers, a National Science Foundation supported Center for Chemical Innovation (CHE-1136607) for financial support of this research.

■ REFERENCES

(1) Wu, J. C.; Yu, T. L.; Chen, C. T.; Lin, C. C. *Coord. Chem. Rev.* **2006**, *250*, 602−626.

(2) Dechy-Cabaret, O.; Martin-Vaca, B.; Bourissou, D. *Chem. Rev.* **2004**, *104*, 6147−6176.

(3) Stanford, M. J.; Dove, A. P. *Chem. Soc. Rev.* **2010**, *39*, 486−494.

(4) Pounder, R. J.; Dove, A. P. *Polym. Chem.* **2010**, *1*, 260−271.

(5) O'Keefe, B. J.; Hillmyer, M. A.; Tolman, W. B. *J. Chem. Soc., Dalton Trans.* **2001**, 2215−2224.

(6) (a) Marshall, E. L.; Gibson, V. C.; Rzepa, H. S. *J. Am. Chem . Soc.* **2005**, *127*, 6048−6051. (b) Dove, A. P.; Gibson, V. C.; Marshall, E. L.; Rzepa, H. S.; White, A. J. P.; Williams, D. J. *J. Am. Chem. Soc.* **2006**, *128*, 9834−9843.

(7) Chisholm, M. H.; Gallucci, J. C.; Quisenberry, K. T.; Zhou, Z. *Inorg. Chem.* **2008**, *47*, 2613−2624.

(8) Bhaw-Luximon, A.; Jhurry, D.; Spassky, N. *Polym. Bull.* **2000**, *44*, 31−38.

(9) Tang, Z.; Gibson, V. C. *Eur. Polym. J.* **2007**, *43*, 150−155.

(10) Hormnirun, P.; Marshall, E. L.; Gibson, V. C.; White, A. J. P.; Williams, D. J. *J. Am. Chem. Soc.* **2004**, *126*, 2688−2689.

(11) Hormnirun, P.; Marshall, E. L.; Gibson, V. C.; Pugh, R. I.; White, A. J. P. *Proc. Natl. Acad. Sci. (USA)* **2006**, *103*, 15343−15348.

(12) Gregson, C. K. A.; Blackmore, I. J.; Gibson, V. C.; Long, N. J.; Marshall, E. L.; White, A. J. P. *Dalton Trans.* **2006**, 3134−3140.

(13) Wu, J.; Chen, Y.-Z.; Hung, W.-C.; Lin, C.-C. *Organometallics* **2008**, *27*, 4970−4978.

(14) Chisholm, M. H. *Inorg. Chim. Acta* **2009**, *362*, 4284−4290.

(15) Poirier, V.; Roisnel, T.; Carpentier, J.-F.; Sarazin, Y. *Dalton Trans.* **2009**, 9820−9827.

(16) Börner, J.; Flörke, U.; Glöge, T.; Bannenberg, T.; Tamm, M.; Jones, M. D.; Döring, A.; Kuckling, D.; Herres-Pawlis, S. *J. Mol. Catal. A* **2010**, *316*, 139−145.

(17) Alcazar-Roman, L. M.; O'Keefe, B. J.; Hillmyer, M. A.; Tolman, W. B. *Dalton Trans.* **2003**, 3082−3087.

(18) Amgoune, A.; Thomas, C. M.; Roisnel, T.; Carpentier, J.-F. *Chem.—Eur. J.* **2006**, *12*, 169−179.

(19) Breyfogle, L. E. Ph.D. Thesis, University of Minnesota: 2005.

(20) The ligand with R = NO_2 was reported in ref 17, but subsequent work indicated that it was not appropriately identified; the synthesis and characterization reported here supersedes that work.

(21) Williams, C. K.; Breyfogle, L. E.; Choi, S. K.; Nam, W.; Young, V. G., Jr.; Hillmyer, M. A.; Tolman, W. B. *J. Am. Chem. Soc.* **2003**, *125*, 11350−11359.

(22) Diffusion constant = 9.650(9) × 10−10 m^2s^{-1}, derived molecular radius = 5.4(3) Å, estimated molecular radius from the X-ray structure = 5.9(5) Å. See refs 19 and 21.

(23) Duda, A.; Penczek, S. *Macromolecules* **1990**, *23*, 1636−1639.

(24) These conditions differ from those used in previous kinetics studies of **1**−**3** reported in refs 17 and 19, where $[CL]_0$ = 1.0 M was used at 25 °C.

(25) Hoops, S.; Sahle, S.; Gauges, R.; Lee, C.; Pahle, J.; Simus, N.; Singhal, M.; Xu, L.; Mendes, P.; Kummer, U. *Bioinformatics* **2006**, *22*, 3067−3074.

(26) Colby, D. A.; Bergman, R. G.; Ellman, J. A. *J. Am. Chem. Soc.* **2008**, *130*, 3645−3651.

(27) (a) Blackmond, D. *Angew. Chem., Int. Ed.* **2005**, *44*, 4302−4320. (b) Mathew, J.; Klussmann, M.; Iwamura, H.; Valera, F.; Futran, A.; Emanuelsson, E.; Blackmond, D. *J. Org. Chem.* **2006**, *71*, 4711−4722.

(28) Addison, A. W.; Rao, T. N.; Reedijk, J.; Rijn, J. v.; Verschoor, G. C. *J. Chem. Soc., Dalton Trans.* **1984**, 1349−1356.

(29) Hansch, C.; Leo, A.; Taft, R. W. *Chem. Rev.* **1991**, *91*, 165−195.

(30) The rate constants used in the Hammett plots of $\log(k_2)$ or $\log(K_M)$ vs σ_p that were not determined directly from the data were extrapolated from the thermodynamic parameters obtained from the Erying (k_2) and van't Hoff (K_M) plots (Table 3, column 4).

(31) Meier, M.; Basolo, F.; Pearson, R. G. *Inorg. Chem.* **1969**, *8*, 795−801.

(32) Barroso, S.; Adão, P.; Madeira, F.; Duarte, M. T.; Pessoa, J. C.; Martins, A. M. *Inorg. Chem.* **2010**, *49*, 7452−7463.

(33) Labourdette, G.; Lee, D. J.; Patrick, B. O.; Ezhova, M. B.; Mehrkhodavandi, P. *Organometallics* **2009**, *28*, 1309−1319.

(34) (a) Toupance, T.; Duberley, S. R.; Rees, N. H.; Tyrrell, B. R.; Mountford, P. *Organometallics* **2002**, *21*, 1367−1382. (b) Yann, S.;

Ruth, H. H.; David, L. H.; Simon, M. H.; Manfred, B. *Dalton Trans.* **2006**, *2*, 340−350.
(35) Michel, F.; Hamman, S.; Philouze, C.; Del Valle, C. P.; Saint-Amana, E.; Thomas, F. *Dalton Trans.* **2009**, 832−842.
(36) Zhao, Y.; Truhlar, D. G. *J. Chem. Phys.* **2006**, *125*, 194101−194118.
(37) Hehre, W. J.; Radom, L.; Schleyer, P. v. R.; Pople, J. A. *Ab Initio Molecular Orbital Theory*; Wiley: New York, 1986.
(38) Cramer, C. J. *Essentials of Computational Chemistry: Theories and Models*, 2nd ed.; John Wiley & Sons: Chichester, U.K., 2004.
(39) Zhao, Y.; Truhlar, D. G. *Theor. Chem. Acc.* **2008**, *120*, 215−241.
(40) (a) Zhao, Y.; Truhlar, D. G. *Acc. Chem. Res.* **2008**, *41*, 157−167. (b) Zhao, Y.; Truhlar, D. G. *J. Chem. Theory Comput.* **2009**, *5*, 324−333.
(41) Marenich, A. V.; Cramer, C. J.; Truhlar, D. G. *J. Phys. Chem. B* **2009**, *113*, 6378−6396.
(42) Frisch, M. J.; Trucks, G. W.; Schlegel, H. B.; Scuseria, G. E.; Robb, M. A.; Cheeseman, J. R.; Scalmani, G.; Barone, V.; Mennucci, B.; Petersson, G. A.; Nakatsuji, H.; Caricato, M.; Li, X.; Hratchian, H. P.; Izmaylov, A. F.; Bloino, J.; Zheng, G.; Sonnenberg, J. L.; Hada, M.; Ehara, M.; Toyota, K.; Fukuda, R.; Hasegawa, J.; Ishida, M.; Nakajima, T.; Honda, Y.; Kitao, O.; Nakai, H.; Vreven, T.; Montgomery, J. A.; Peralta, J. E.; Ogliaro, F.; Bearpark, M.; Heyd, J. J.; Brothers, E.; Kudin, K. N.; Staroverov, V. N.; Kobayashi, R.; Normand, J.; Raghavachari, K.; Rendell, A.; Burant, J. C.; Iyengar, S. S.; Tomasi, J.; Cossi, M.; Rega, N.; Millam, J. M.; Klene, M.; Knox, J. E.; Cross, J. B.; Bakken, V.; Adamo, C.; Jaramillo, J.; Gomperts, R.; Stratmann, R. E.; Yazyev, O.; Austin, A. J.; Cammi, R.; Pomelli, C.; Ochterski, J. W.; Martin, R. L.; Morokuma, K.; Zakrzewski, V. G.; Voth, G. A.; Salvador, P.; Dannenberg, J. J.; Dapprich, S.; Daniels, A. D.; Farkas, Ö.; Foresman, J. B.; Ortiz, J. V.; Cioslowski, J.; Fox, D. J. *Gaussian 09, Revision A.02*; Gaussian, Inc.: Wallingford, CT, 2010.